Non-Resonant Multipactor - A Statistical Model

J. Rasch[1], *J. F. Johansson*[2]

1) Chalmers University of Technology, Göteborg, Sweden,

joel.rasch@chalmers.se

2) RUAG Space AB, Göteborg, Sweden

Abstract

High power microwave systems operating in vacuum or near vacuum run the risk of multipactor breakdown. In order to avoid multipactor, it is necessary to make theoretical predictions of critical parameter combinations. These treatments are generally based on the assumption of electrons moving in resonance with the electric field while traversing the gap between critical surfaces. Through comparison with experiments, it has been found that only for small system dimensions will the resonant approach give correct predictions. Apparently, the resonance is destroyed due to the statistical spread in electron emission velocity, and for a more valid description it is necessary to resort to rather complicated statistical treatments of the electron population, and extensive simulations. However, in the limit where resonance is completely destroyed it is possible to use a much simpler treatment, here called non-resonant theory. In this paper we develop the formalism for this theory, use it to calculate universal curves for the existence of multipactor, and compare with previous results. Two important effects that leads to an increase in the multipactor threshold in comparison with the resonant prediction are identified. These are the statistical spread of impact speed, which leads to a lower average electron impact speed, and the impact of electrons in phase regions where the secondary electrons are immediately reabsorbed, leading to an effective removal of electrons from the discharge.

I. INTRODUCTION

Multipactor is a serious failure mechanism for high power RF systems working in vacuum or near vacuum conditions[1,2]. The multipactor discharge consists of electrons that move between conducting surfaces, being accelerated by the electric field and causing secondary electron emission upon impact. Under suitable conditions, the number of electrons will grow exponentially in time and eventually saturate due to space charge effects. The oscillating cloud of electrons formed in the system will create noise and disturb the signals in various ways, but what is an even greater risk is that the impact of electrons on the surfaces might lead to significant outgassing and subsequent corona breakdown.

In order to avoid multipactor discharges, different theoretical models have been used over the past decades. They are typically based on the dynamics of electrons moving in a homogeneous electric field between two large parallel plates[3], and for electrons to participate in the multipactor avalanche, they must fulfill certain resonance criteria with respect to emission and impact times. However, this model is only applicable in systems where the gap size is small, and the spread in emission velocities of the electrons is small. This was realized quite early[4], when the predicted resonance bands were only found for the first couple of modes of resonance. For higher modes, the resonance bands tend to merge into a continuum with rather small variations.

Another complication is added when one tries to apply the resonant model to more complicated geometries than the parallel plates. Only in a few cases[5–14] can the problem be treated analytically. This has motivated the wide use of numerical simulations, both particle-in-cell (PIC) and Monte Carlo, to calculate the breakdown thresholds and study the electron trajectories. The numerical simulation approach has a major drawback; for complicated and large systems, it is necessary to use a great number of electrons and long simulation times. Since there are certain stochastic elements in the codes (typically emission velocities) there is also the problem of reproduciblity, and thus many simulations are needed to find an accurate breakdown threshold.

The resonant model is only valid when the spread in emission velocity, and the gap size is small. When the emission spread and gap size becomes larger, resonance is destroyed, and any analytical approach to the problem needs to be based on statistical methods.

Rather recently[15], a sophisticated statistical approach to calculate the threshold and elec-

tron dynamics has been developed. It takes into account the statistical spread in impact time for electrons, depeding on the emission phase and speed. The electron population is tracked by developing a sequence of integral equations. This model is very precise, and has shown excellent agreement with simulations, but suffers from the drawback of being rather complicated, since it is necessary to evaluate the transfer probability functions exactly through a rather elaborate scheme. For complicated structures this process becomes extremely complex. For this reason, the statistical approach has so far only been applied to double-sided multipactor between parallel plates[15–18], in a rectangular waveguide[19], and single-sided multipactor on a dielectric surface[20]. The theory has also recently been generalized to multicarrier signals, again in the parallel plates geometry[21]. Unfortunately, it is not obvious how to apply it to more complicated geometries.

Since the recent statistical methods are valid for any gap size and velocity spread, the mathematical formulation is rather involved. However, in the limit when the velocity spread and gap size are sufficiently large, the impact phase of an electron will be almost independent of its emission phase, and the electrons can be assumed to be evenly distributed in space above the surface of impact. We here call this type of multipactor non-resonant, and in a sense, it can be viewed as one of the two extremes of the full statistical model above. The limit for small gaps and velocity spreads corresponds to the resonant model, whereas the limit for large gaps and velocity spreads corresponds to the non-resonant model. In the non-resonant limit, the complexity of the problem is reduced significantly, which allows for rapid calculations. The main qualitative difference between the resonant and non-resonant model is that in the non-resonant model, the electrons will be impacting over the entire field period, with the electron number and impact speed having a certain statistical spread. This leads to a lower average impact speed than in the resonant case, which raises the breakdown threshold. However, more importantly, it also leads to the effective loss of electrons when they impact in phase regions where the secondary electrons are directly pushed back into the surface. This leads to a loss of electrons into low energy single side multipactor, and an effective removal of electrons from the discharge process. This electron sink can under certain conditions remove up to half of the impacting electron number, which significantly raises the necessary voltage and secondary emission yield (SEY) maximum that is needed to cause breakdown in comparison to resonant multipactor.

In this paper we develop a simplified theoretical model of the impact and emission statis-

tics of the electrons in the initial discharge stage (no space charge effects) that we call the non-resonant model[22]. It enables fast evaluation of the breakdown threshold and impact statistics for systems where the electrons are expected to move non-resonantly. The fundamental assumption which renders the analysis less complex as compared to the full statistical treatment is that the electrons involved in the discharge are assumed to be evenly distributed in space above the surface of impact. This assumption is valid when the spread in emission velocity is sufficiently large, and the electron trajectories are sufficiently long. This approach is by no means new. Several papers published in the Soviet Union in the 70's used the assumption of evenly distributed electrons, typically calling it the polyphase regime, and derived the corresponding impact probabilities[23–27]. Recently, the polyphase approach has received renewed interest in connection with experiments on single-sided multipactor[28]. For small gap sizes, the velocity spread will cause no disturbance to the resonance, and high energy impacts will be caused by the electrons that are emitted with the highest energy. In this way, only the electrons that correspond to a certain resonance band will be involved in the breakdown. However, when the gap size becomes larger, the emission velocity spread will cause this linking between emission and impact phase to be destroyed, meaning that it is no longer the most energetic electrons that are solely responsible for the discharge, but also low energy emission electrons will be causing high energy impacts. This will lead to the participation in the discharge of electrons emitted from a wider phase band than in the resonant case. In the susceptibility diagram this is seen as the expansion of the resonance bands to the sides, causing them to blur. In reality, for large enough gaps, there will be a contribution from all electrons with a positive drift velocity (although the influence of slow electrons is limited due to the long gap transit times as compared with the fast electrons), and the term polyphase seems a bit misleading. Instead we prefer to call it by one of the other names in use: non-resonant multipactor. In any case, the assumption was the same, and most of the key results were found, but the investigations were severly limited by the computer power available, and the secondary electron emission models in use at the time. For example, Grishin and Luk'yanchikov[26] found that by using the non-resonant approach, and an approximation for the SEY curve, there could be no multipactor if the SEY maximum was below 1.96. Their conclusion about a lower value for the SEY maximum which will allow multipactor was correct, but the accuracy was limited by the precision in the numerical calculations, and the fact that the treatment did not incorporate single sided electron

multiplication.

With present computers and programs, the implementation of the non-resonant model is rather easy, and the computation time needed is measured in seconds. The great speed of the calculations as compared to simulations is due to the elimination of the long electron trajectories by making the impact and emission statistics a purely local process. This hopefully signals the possible application of the statistical approach to more complicated systems, where the need for evaluating the transfer probability function exactly is removed. The inhomogeneity of the electric field can be incorporated using the concept of the ponderomotive force, which affects the electron drift velocity[10,20,28–30], and the concept of geometrical spreading can be used to model curved surfaces by diluting the electron density appropriately[29].

II. ELECTRON DYNAMICS

In this section we rederive the emission and impact characteristics of electrons involved in the multipactor discharge. We shall see that the field oscillation period can be divided into a segment corresponding to electrons that will move away from the surface until returned by some external force, and another segment where the emitted electrons will impact the surface again within one period from emission. The electron population can at all times be divided into these two populations, the "long range" and "short range" electrons. The long range electrons are able to move between surfaces in the system, and the dynamics of their motion is assumed to be dictated by the geometry of the metal or dielectric surfaces, coupled with the action of RF ponderomotive forces and applied external DC electric and magnetic fields. To simplify the treatment in this paper, we shall assume that the field gradients and surface curvatures are small enough to be neglected, and the emission and impact surfaces can be considered as locally flat, with an electric field that is normal to the surface, and homogeneous. The field can be considered as homogeneous, and the surface can be considered as flat if two conditions are fulfilled. First, the electron oscillation amplitude should be much smaller than the scale length of the gradient of the electric field, and second; the electron oscillation amplitude should be much larger than the scale length of irregularity of the surface.

A. Electron Emission

Consider a conductive surface subject to an oscillating electric field which is parallel to the surface normal, $\hat{z}$. Under these conditions, the field is described by

$$\bar{E} = \hat{z} E_0 \sin \omega t \tag{1}$$

where E_0 is the amplitude of the electric field, ω the field angular frequency, and t the time. The motion of an electron in this field , when the electron velocity is small in comparison with the speed of light, is described by

$$\ddot{z} = -\frac{eE_0}{m} \sin \omega t \tag{2}$$

where e is the electron charge, and m the electron mass. If we consider an electron which is emitted from the surface ($z = 0$) at the time t_e with an initial velocity, v_e, in the z-direction, we find the trajectory, $z(t)$, and velocity, $v(t)$

$$z(t) = \frac{v_\omega}{\omega}(\sin \omega t - \sin \omega t_e) + (v_e - v_\omega \cos \omega t_e)(t - t_e) \tag{3}$$

$$v(t) = v_\omega(\cos \omega t - \cos \omega t_e) + v_e \tag{4}$$

where $v_\omega \equiv eE_0/(m\omega)$ is the amplitude of the oscillatory velocity. The electron emission velocity, v_e, is a quantity with a certain statistical spread. In fact, this is the foundational hypothesis of the non-resonant approach. However, in our treatment, we do not include the spread explicitly, we simply assume that it is large enough to cause nonresonance. Of course, this means that the theory will only be exact when $\Delta v_e \ll v_e$, where Δv_e is the typical spread in the emission velocity. This in turn requires very large electron transit times, for the discharge to become non-resonant (see section III). In reality, most surface materials will have $\Delta v_e \approx v_e$, which makes it unclear how good the predictive power of the theory will be with respect to real multipactor discharges. However, taking into account the effect of a more realistic emission velocity spread goes beyond the scope of this paper.

It is clear that the initial acceleration imparts a drift velocity to the electron

$$v_d = v_e - v_\omega \cos \omega t_e \tag{5}$$

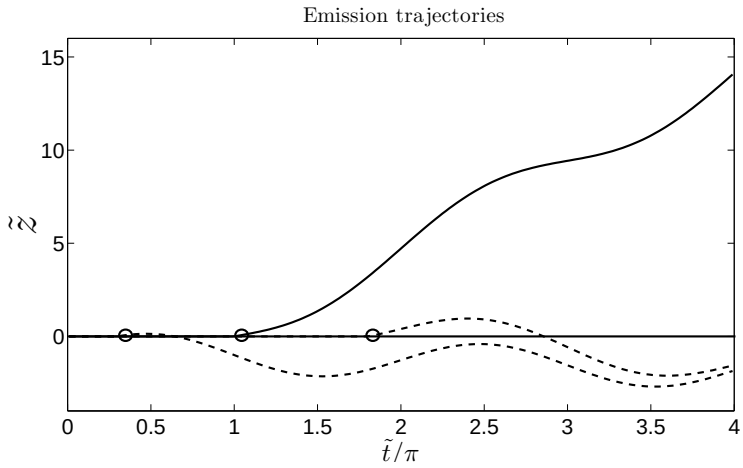

FIG. 1: This figure illustrates the importance of emission phase for the future motion of an emitted electron. The dashed curves represent electrons emitted at a phase which leads to reabsorbtion, whereas the solid curve represents an electron that is able to leave the plane (symbolized by the straight line).

which depends strongly on the emission time. For convenience we introduce the normalized variables $\tilde{t} \equiv \omega t$, $\tilde{z} \equiv \omega z/v_\omega$, $\alpha \equiv v_e/v_\omega$, and $\tilde{v}(\tilde{t}) \equiv \partial\tilde{z}/\partial\tilde{t}$. The equations for the motion of the electron after emission become

$$\begin{aligned} \tilde{z}(\tilde{t}) &= \sin\tilde{t} - \sin\tilde{t}_e + (\alpha - \cos\tilde{t}_e)(\tilde{t} - \tilde{t}_e) \\ \tilde{v}(\tilde{t}) &= \cos\tilde{t} + \alpha - \cos\tilde{t}_e = \cos\tilde{t} + \tilde{v}_d \end{aligned} \tag{6}$$

It is very important to realize that electrons that are emitted with certain values for the emission phase $\tilde{t}_e$ will return to the surface within one period. These are the short range electrons. We can find the values for the emission phase when this happens by solving

$$\begin{aligned} &\tilde{z}(\tilde{t}_e + \tilde{t}_i) < 0 \\ &0 \leq \tilde{t}_i \leq 2\pi \end{aligned} \tag{7}$$

where $\tilde{t}_i$ is the impact time. The limits for short range emission are illustrated in Fig. 2.

The electrons that are not short range will drift away from the surface, and will only return due to some external force, for example the ponderomotive force of an electric inhomogeneity[10,19,29]. These are the long range electrons.

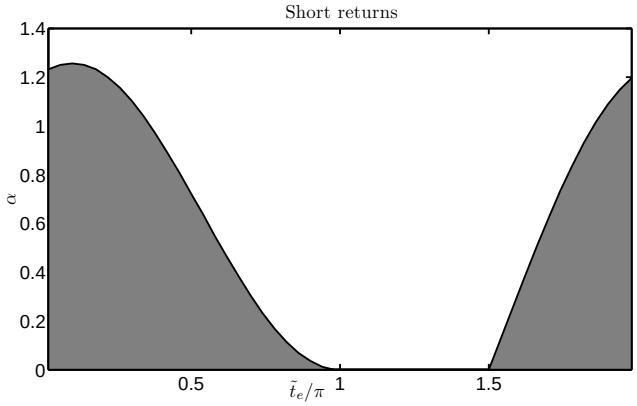

FIG. 2: The limiting times for long range electron emission as a function of the normalized emission velocity α. Grey area represents short range emission, and white long range.

B. Long Range Impacts

We will now consider the impact dynamics of long range electrons, and determine limiting impact times and heights for electrons as functions of their drift speed. The drift speed is set by the emission velocity and phase. In the case of single-sided multipactor in coaxial and circular waveguides excited in the TE_{01} and TM_{01} modes respectively, electrons are reflected by the ponderomotive force while approaching the center, and therefore return towards the emitting surface with their drift velocity reversed. In the case of parallel plates of the same material, the drift velocity of electrons approaching one plate is determined by the emission phase at the opposing plate. But in the non-resonant limit, the impact dynamics are determined completely by the drift speed of the electrons, and considerations about detailed trajectories and emission phases are unnecessary. This allows us to treat the impact dynamics by only looking at one surface. And in a steady state scenario, the two opposing plates will spawn secondaries with the exact same distribution over the magnitude of the drift velocity.

Thus, we consider impacts on the surface located at $\tilde{z} = 0$, in this case, only long range electrons that drift in the negative z-direction will be able to impact. The full motion of the electrons is made up of an oscillatory part, determined by the local field at the surface, and the drift part (see Eq. (6)). The electrons move according to (assuming $\tilde{v}_d$ is positive)

$$\tilde{v}(\tilde{t}) = \cos\tilde{t} - \tilde{v}_d \tag{8}$$

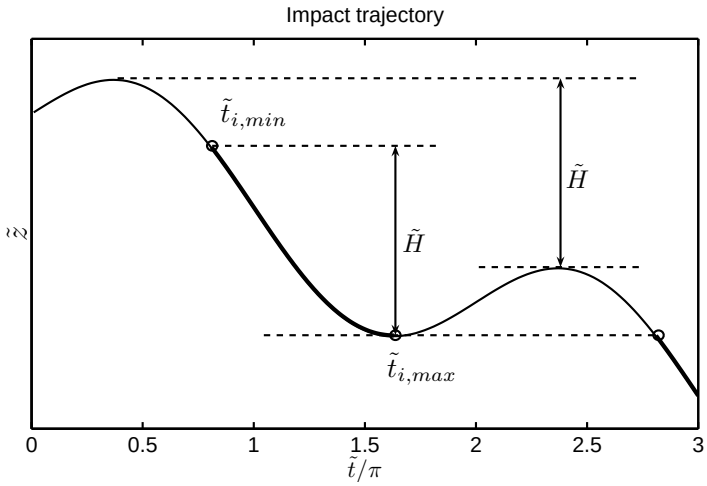

FIG. 3: Relevant features of the approaching trajectories. The circles mark the limiting phases for impact, and $\tilde{H}$ is the normalized distance the electron drifts during one period, i.e. $\tilde{H} = 2\pi\tilde{v}_d$.

By integrating this equation and setting the height above the surface at $\tilde{t} = 0$ to $\tilde{h}$, we find the trajectory

$$\tilde{z}(\tilde{t}) = \sin\tilde{t} - \tilde{v}_d\tilde{t} + \tilde{h} \tag{9}$$

In Fig. 3 the important features of approaching trajectories are shown. It is clear that if $\tilde{v}_d < 1$, there are two limiting values for the impact time, $\tilde{t}_{i,\min}$ and $\tilde{t}_{i,\max}$, below and above which impact is impossible during one period. An electron which did not suffer impact during the first period will start from a lower position at the beginning of the next period. The height of this new position is the original height, $\tilde{z}(0) = \tilde{h}$, minus the distance the electron drifts during one cycle, $\tilde{H} = 2\pi\tilde{v}_d$. Thus $\tilde{z}(2\pi) = \tilde{h} - \tilde{H} = \tilde{h} - 2\pi\tilde{v}_d$.

The limiting values for the impact times can be found as a function of the normalized drift velocity and the initial height, provided that the normalized drift velocity is less than unity and larger than zero. Along with the minimum and maximum time of impact there is a minimum and maximum height: $\tilde{h}_{\min}$ and $\tilde{h}_{\max}$, from where these electrons start. The maximum time of impact is located at the middle circle in Fig. 3, where the motion of the electron is reversed, and the velocity, $\tilde{v}$, is zero. It is clear that this can only happen when $\tilde{t}_i \geq 3\pi/2$, and from Eq. (8) We find

$$\tilde{v}(\tilde{t}_{i,\max}, \tilde{v}_d) = 0 \quad \Rightarrow \quad \tilde{t}_{i,\max} = 2\pi - \arccos(\tilde{v}_d) \tag{10}$$

If the starting height of an electron is too high, the electron motion will reverse before it reaches the surface, i.e. $\tilde{z}(\tilde{t}_{i,\max}) > 0$. The limiting height is thus found by using Eqs. (9) and (10), and solving for $\tilde{z}(\tilde{t}_{i,\max}) = 0$,

$$\tilde{h}_{\max} = \sin(\arccos(\tilde{v}_d)) + \tilde{v}_d(2\pi - \arccos(\tilde{v}_d)) \tag{11}$$

There is also a minimum height, located at a point $\tilde{h}_{\max} - \tilde{H} = \tilde{h}_{\max} - 2\pi\tilde{v}_d$. The reason for this is that the region below this height will have been cleared of electrons during the previous period due to impacts with the surface. Using Eq. (11) we find

$$\tilde{h}_{\min} = \tilde{h}_{\max} - 2\pi\tilde{v}_d = \sin(\arccos(\tilde{v}_d)) - \tilde{v}_d \arccos(\tilde{v}_d) \tag{12}$$

The minimum time of impact, $\tilde{t}_{i,\min}$, correspond to the time of impact of an electron starting at $\tilde{h}_{\min}$. It is found by inserting $\tilde{h} = \tilde{h}_{\min}$ in (9) and solving for $\tilde{z}(\tilde{t}_{i,\min}) = 0$, viz.

$$\tilde{v}_d\tilde{t}_{i,\min} - \sin(\tilde{t}_{i,\min}) = \tilde{h}_{\min} \tag{13}$$

The solutions to Eqs. (10), (11), (12) and (13) must in general be found numerically, and only in the two cases when $\tilde{v}_d = 0$ and $\tilde{v}_d = 1$ do we find analytical limits, which are shown in table 1.

	$\tilde{v}_d = 0$	$\tilde{v}_d = 1$
$\tilde{t}_{i,\min}$	$3\pi/2$	0
$\tilde{t}_{i,\max}$	$3\pi/2$	2π
$\tilde{h}_{\min}$	1	0
$\tilde{h}_{\max}$	1	2π

Table 1. The analytical limits for the minimum and maximum impact times and heights corresponding to normalized drift speeds zero and unity.

These limits make perfect intuitive sense. When the drift velocity is zero, the electrons will have no net drift towards the surface, and although an electron that would be within the normalized distance 1 from the surface would impact during a cycle, there would only be

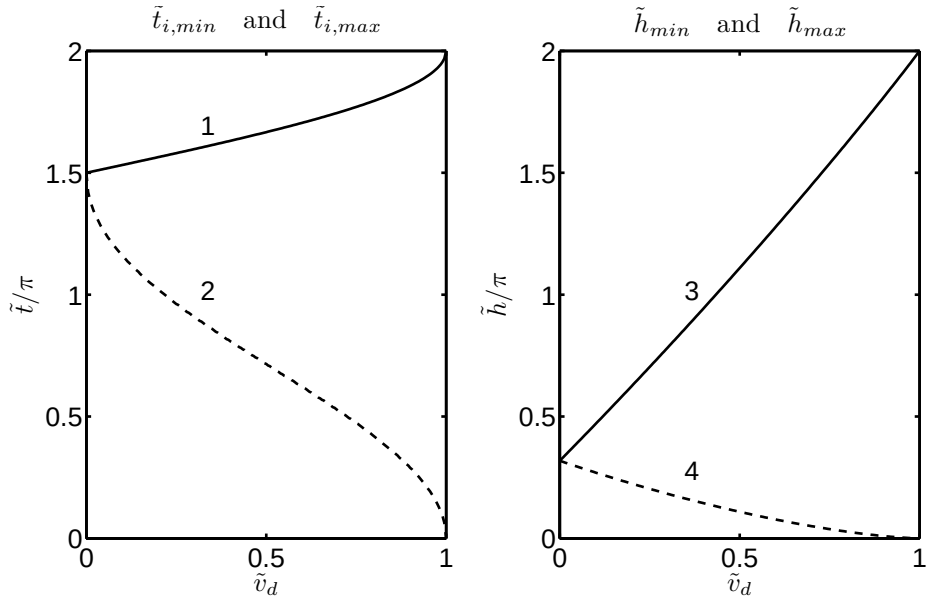

FIG. 4: The minimum and maximum impact times and heights as functions of the drift velocity. Lines 1 and 2 represent the maximum and minimum impact time respectively, whereas lines 3 and 4 represent the maximum and minimum impact height.

impacts during that cycle, and afterwards all electrons would be gone. This is the reason for the joining of the maximum and minimum height at the value 1 in the limit where $\tilde{v}_d = 0$. In the opposite case, when $\tilde{v}_d = 1$, the height over which electrons are impacting during a field period extends from 0 to 2π, and electrons will impact during the entire period. The limiting times and heights as a function of the drift velocity can be seen in Fig. 4.

It is also necessary to know the minimum drift velocity that is able to cause impact for a given impact phase, $\tilde{t}_i$. When $\tilde{t}_i \geq 3\pi/2$ this corresponds to the drift velocity which causes reversal of the electron motion at $\tilde{t}_i$. Thus, the minimum drift velocity, $\tilde{v}_{d,\min}$, that can cause impact at a certain $\tilde{t}_i$ is given by the solution of $\tilde{v}(\tilde{t}_i, \tilde{v}_{d,\min}) = 0$. From (8)

$$\tilde{v}(\tilde{t}_i, \tilde{v}_{d,\min}) = 0 \quad \Leftrightarrow \quad \tilde{v}_{d,\min} = \cos \tilde{t}_i \tag{14}$$

and when $\tilde{t}_i < 3\pi/2$, the minimum drift velocity corresponds simply to the electrons that start from the minimum height, given by Eq. (12), that cause impact at the instant $\tilde{t}_i$. So from Eq. (9), the minimum drift velocity is found by solving

$$\tilde{v}_{d,\min}\tilde{t}_i - \sin(\tilde{t}_i) = \tilde{h}_{\min}(\tilde{v}_{d,\min}) \tag{15}$$

III. IMPACT STATISTICS

In this section we derive the impact statistics of non-resonant, long range electrons moving towards a surface. The non-resonant limit is reached when the emission velocity spread is large enough to cause the time of arrival for the most energetic electrons that are approaching the surface to be completely randomized. To determine when this approximation applies, consider electrons that are emitted with the highest drift velocity from a surface. At first the electrons will form a thin sheath moving away from the surface, but as they drift, the velocity spread will cause the electron sheath to expand. When the sheath has expanded to a size that is larger than the distance the electrons can drift during one period, electrons emitted from different cycles will start to mix with each other and form a continuous cloud moving away from the surface. This is the essence of the non-resonant approximation, and it is valid when the drift velocity spread times the flight time is larger than the drift speed times the field period. For the fastest electrons, $v_d \approx v_e + v_\omega$, which means

$$\Delta v_e P \frac{2\pi}{\omega} > (v_e + v_\omega)\frac{2\pi}{\omega} \tag{16}$$

where P is the number of field periods since the time of emission. In a parallel plate system, the gap width d is traversed in roughly $P \approx d\omega/(2\pi(v_e + v_\omega))$ periods, giving

$$\Delta v_e d > \frac{2\pi}{\omega}(v_e + v_\omega)^2 \tag{17}$$

In Fig. 5 the electron spreading due to the emission velocity spread is illustrated. In this example, the emission velocity is assumed to follow a normal (Gaussian) distribution, with a standard deviation $\sqrt{\langle \Delta v_e^2 \rangle} = 0.025 v_d$. According to (17), this value of emission velocity spread implies that the non-resonant regime should be reached when $d\omega/(2\pi v_d) > 40$, but it is clear from the figure that the mixing of the consecutive electron bunches becomes significant far before this.

Assuming that the non-resonant criterion is fulfilled, we now proceed to derive the impact statistics. Instead of considering one electron coming towards the surface, we wish to determine the impact distribution of a large number of electrons, moving towards the surface, with different drift velocities. The easiest way to derive the mathematical relationships is to start with a bunch of long range electrons having a single drift velocity, and assume that there are N_l electrons over the surface which will impact during the next cycle. Since we are

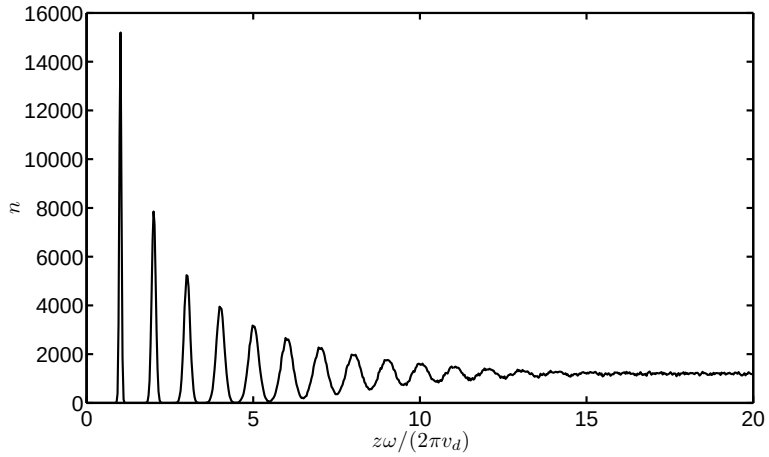

FIG. 5: The density, n, of electrons above an emitting surface, located at $z = 0$. The emission velocity distribution is normal (Gaussian) with a standard devioation $\sqrt{\langle \Delta v_e^2 \rangle} = 0.025 v_d$, and a mean which is v_d. During each field period a bunch consisting of 40000 electrons is emitted at a fixed emission phase. As the bunches move away from the surface, the individual position of each electron becomes displaced from the average position, which results in the mixing of the consecutive bunches.

assuming complete nonresonance, these electrons will be evenly distributed over a segment of length $\tilde{H} = 2\pi\tilde{v}_d$, extending from $\tilde{h}_{\min}$ to $\tilde{h}_{\max}$. The density of electrons over the surface, n_l, is thus a constant in that height interval

$$n_l = \frac{N_l}{\tilde{H}} = \frac{N_l}{2\pi\tilde{v}_d} \tag{18}$$

These electrons will impact in an interval $\tilde{t}_i \in [\tilde{t}_{i,\min}, \tilde{t}_{i,\max}]$, and give rise to an impact density, $n_{i,l}(\tilde{t}_i)$, related to n_l through

$$n_{i,l}(\tilde{t}_i)d\tilde{t}_i = n_l d\tilde{h} \tag{19}$$

Corresponding to each impact time, for a given drift velocity, there is a unique height, $\tilde{h}(\tilde{t}_i)$ from where the electron starts at $\tilde{t} = 0$. From Eq. (9) we find

$$\tilde{h}(\tilde{t}_i) = \tilde{v}_d\tilde{t}_i - \sin\tilde{t}_i \tag{20}$$

and consequently

$$d\tilde{h}(\tilde{t}_i) = (\tilde{v}_d - \cos\tilde{t}_i)d\tilde{t}_i \tag{21}$$

Combining this result with (18) and (19) gives

$$n_{i,l}(\tilde{t}_i)d\tilde{t}_i = n_l(\tilde{v}_d - \cos\tilde{t}_i)d\tilde{t}_i = \frac{N_l}{2\pi\tilde{v}_d}(\tilde{v}_d - \cos\tilde{t}_i)d\tilde{t}_i \tag{22}$$

In order to describe the non-resonant discharge, we need to take be able to take into account electrons having different drift velocities. The incoming long range electrons are distributed over normalized drift velocity and height, so we introduce a distribution function, $\eta_l(\tilde{h}, \tilde{v}_d)$, which integral over drift velocity gives the electron density at a specific height. So

$$n_l(\tilde{h}) = \int_{\tilde{v}_{d,\min}}^{\infty} \eta_l(\tilde{h}, \tilde{v}_d)d\tilde{v}_d \tag{23}$$

where $\tilde{v}_{d,\min}$ is given by the solution to Eq. (15). Furthermore, the density of incoming electrons in velocity space is found by integrating over normalized height

$$n_l(\tilde{v}_d) = \int_{\tilde{h}_{\min}}^{\tilde{h}_{\max}} \eta_l(\tilde{h}, \tilde{v}_d)d\tilde{h} \tag{24}$$

But the non-resonant assumption states that electrons are evenly distributed in the height segment $\tilde{H} = \tilde{h}_{\max} - \tilde{h}_{\min} = 2\pi\tilde{v}_d$ above the surface. This means that

$$n_l(\tilde{v}_d) = \int_{\tilde{h}_{\min}}^{\tilde{h}_{\max}} \eta_l(\tilde{h}, \tilde{v_d})d\tilde{h} = 2\pi\tilde{v}_d\eta_l(\tilde{h}, \tilde{v}_d) \quad \Leftrightarrow \quad \eta_l(\tilde{h}, \tilde{v}_d) = \frac{n_l(\tilde{v}_d)}{2\pi\tilde{v_d}} \tag{25}$$

The impact density is distributed over normalized impact time and impact speed. Only electrons that are moving towards the surface will impact. Consequently, the normalized impact speed (which is a positive quantity) of the long range electrons is found by changing the sign of Eq. (8)

$$\tilde{v}_{i,l} = -\tilde{v}(\tilde{t}_i) = \tilde{v}_d - \cos\tilde{t}_i \tag{26}$$

We introduce the impact distribution function, $\eta_{i,l}(\tilde{t}_i, \tilde{v}_i)$, caused by the long range electron distribution, η_l. If $\eta_{i,l}$ is integrated over all allowed impact velocities, it gives the impact density, $n_{i,l}(\tilde{t}_i)$, at a specific impact time, $\tilde{t}_i$,

$$n_{i,l}(\tilde{t}_i) = \int_{\tilde{v}_{i,l,\min}}^{\infty} \eta_i(\tilde{v}_{i,l}, \tilde{t}_i)d\tilde{v}_{i,l} \tag{27}$$

where

$$\tilde{v}_{i,l,\min} = \tilde{v}_{d,\min} - \cos\tilde{t}_i \tag{28}$$

Since the relation between $\tilde{v}_{i,l}$ and $\tilde{v}_d$ for a given $\tilde{t}_i$ is linear, we can equally well take $\eta_{i,l}$ to be a function of $\tilde{v}_d$, and take the integral over drift velocity

$$n_{i,l}(\tilde{t}_i) = \int_{\tilde{v}_{d,\min}}^{\infty} \eta_i(\tilde{v}_d, \tilde{t}_i) d\tilde{v}_d \tag{29}$$

In fact, the relationship between the electron distribution in phase space above the surface and the corresponding impact distribution is

$$\eta_{i,l}(\tilde{t}_i, \tilde{v}_{i,l}) d\tilde{t}_i d\tilde{v}_{i,l} = \eta_l(\tilde{h}, \tilde{v}_d) d\tilde{h} d\tilde{v}_d \tag{30}$$

Using $d\tilde{v}_{i,l} = d\tilde{v}_d$, and Eqs. (21) and (25) we find

$$\eta_{i,l}(\tilde{t}_i, \tilde{v}_d) = \frac{n_l(\tilde{v}_d)}{2\pi\tilde{v}_d}(\tilde{v}_d - \cos\tilde{t}_i) \tag{31}$$

It is interesting to investigate the impact distribution of a cloud of electrons all having the same drift velocity, $\tilde{v}_{d,0}$. This would represent the population of electrons emitted at the same phase with a small velocity spread, at first occupying a very thin layer in space. But they have now travelled so far that this thin layer has expanded into a region covering the impact height several periods. If there are N_l electrons that will impact during one cycle, the density in velocity space is given by

$$n_l(\tilde{v}_d) = N_l \delta(\tilde{v}_d - \tilde{v}_{d,0}) \tag{32}$$

where δ is the Dirac delta function. From Eq. (31) we find

$$\eta_{i,l}(\tilde{t}_i, \tilde{v}_d) = \frac{N_l}{2\pi\tilde{v}_d}(\tilde{v}_d - \cos\tilde{t}_i)\delta(\tilde{v}_d - \tilde{v}_{d,0}) \tag{33}$$

and from Eq. (29) the impact density is

$$n_{i,l}(\tilde{t}_i \in [\tilde{t}_{i,\min}, \tilde{t}_{i,\max}]) = \int_{\tilde{v}_{d,\min}}^{\infty} \eta_{i,l}(\tilde{t}_i, \tilde{v}_d) d\tilde{v}_d = \frac{N}{2\pi\tilde{v}_{d,0}}(\tilde{v}_{d,0} - \cos\tilde{t}_i) \tag{34}$$

This impact distribution is seen in Fig. 6 for values of $\tilde{v}_{d,0}$ ranging from 50 to 0.1. In a resonant discharge, all electrons impact at a specific phase, and for certain combinations of gap width and frequency, the electrons impact with the maximum velocity, $v_i = 2v_\omega + v_e$. In

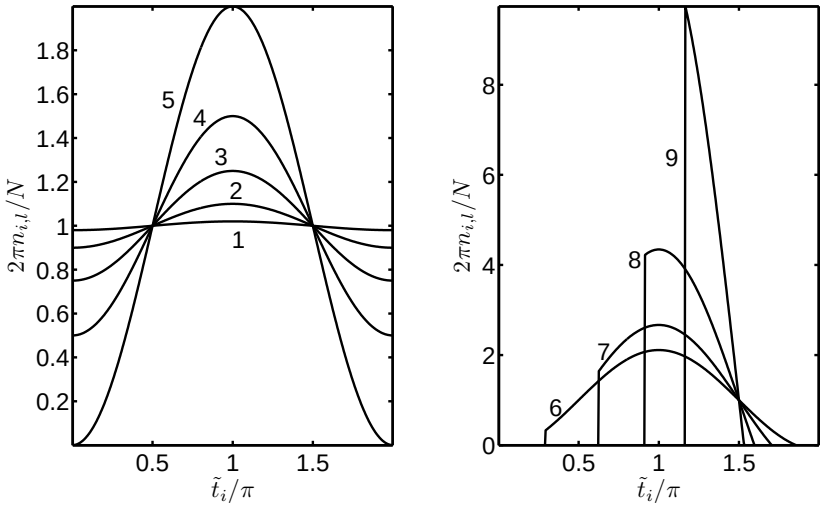

FIG. 6: The impact distribution of a bunch of electrons all having the same drift velocity. Curves 1 to 5 show the impact distributions for $\tilde{v}_d$ equal to 50, 10, 4, 2 and 1. It is clear that when the electrons are not allowed to move resonantly, the spread over impact phases will lead to a lower secondary emission, and a loss of electrons into the short range phase, given that the emission velocity, α, is small. Curves 6 to 9 show the impact distribution of electrons having normalized drift speeds $\tilde{v}_d = 0.9$, 0.6, 0.3, and 0.1. The impact region becomes smaller when the drift speed decreases.

the non-resonant case, the impacts are distributed over a phase region $[\tilde{t}_{i,\min}, \tilde{t}_{i,\max}]$, which means that the average impact speed will always be lower than this value. For low values of $\tilde{v}_{d,0} > 1$, the impact distribution will basically be sinusoidal, which leads to a loss of electrons into short range emission and low energy secondaries (see Fig. 2) but when $\tilde{v}_{d,0}$ is large, the entire field period is open for long range emission, and this loss source is eliminated. For very low values of $\tilde{v}_{d,0}$, the impacts are limited to a small interval between π and $3\pi/2$, giving rise to long range secondaries with a certain spread in drift velocity.

We can also calculate the average impact speed, $\tilde{u}_{i,l}(\tilde{t}_i)$, by multiplying $\eta_{i,l}$ with the impact speed, $\tilde{v}_{i,l} = \tilde{v}_{d,0} - \cos\tilde{t}_i$, and integrating. In this way we find

$$\tilde{u}_{i,l}(\tilde{t}_i \in [\tilde{t}_{i,\min}, \tilde{t}_{i,\max}]) = \frac{\int_{\tilde{v}_{d,\min}}^{\infty} \eta_{i,l}(\tilde{t}_i, \tilde{v}_d)\tilde{v}_{i,l} d\tilde{v}_d}{\int_{\tilde{v}_{d,\min}}^{\infty} \eta_{i,l}(\tilde{t}_i, \tilde{v}_d) d\tilde{v}_d} = \tilde{v}_{d,0} - \cos\tilde{t}_i \tag{35}$$

Which is just the impact speed, $\tilde{v}_{i,l}$.

The total average impact speed, $\tilde{w}_{i,l}$, is found by integrating $\tilde{u}_{i,l}$ over the impact times.

For the case when $\tilde{v}_d \geq 1$, the entire period is the integration domain, and using Eqs. (34) and (35) we find

$$\tilde{w}_{i,l} = \frac{\int_0^{2\pi} n_{i,l}(\tilde{t}_i)\tilde{u}_{i,l}d\tilde{t}_i}{\int_0^{2\pi} n_{i,l}(\tilde{t}_i)d\tilde{t}_i} = \frac{\tilde{v}_{d,0}^2 + \frac{1}{2}}{\tilde{v}_{d,0}} \tag{36}$$

If we switch back to unnormalized variables we find

$$w_{i,l} = \frac{v_{d,0}^2 + \frac{1}{2}v_\omega^2}{v_{d,0}} \tag{37}$$

For electrons having the maximal drift velocity, $v_e + v_\omega$, this becomes

$$w_{i,l} = \frac{(v_\omega + v_e)^2 + \frac{1}{2}v_\omega^2}{v_\omega + v_e} \tag{38}$$

This formula was derived previously[29] in a slightly different way, and used to approximate the average impact speed in a non-resonant discharge.

IV. SHORT RANGE IMPACTS

The previous investigation of impact statistics only dealt with electrons coming from far away, drifting close to the surface, and being randomly distributed in height. If we wish to perform a similar analysis for the short range electrons, we cannot use the non-resonant approach. Short range electrons have as their sole characteristic the emission phase, $\tilde{t}_e$. The emission phase determines completely the impact phase, $\tilde{t}_i$. In fact, it should be sufficient to describe the density of impacting short range electrons, $n_{i,s}$, at $\tilde{t}_i$, as a function of the density of emitted short range electrons, n_s, at $\tilde{t}_e$ using

$$n_{i,s}(\tilde{t}_i)d\tilde{t}_i = n_s(\tilde{t}_e)d\tilde{t}_e \tag{39}$$

The relationship between emission and impact phase is given by a function, f

$$\tilde{t}_i = f(\tilde{t}_e) \tag{40}$$

which symbolizes the connection between normalized emission and impact time, in the short range emission interval, that one finds when solving Eqs. (7). Assuming that f is known we can write

$$n_{i,s}(f(\tilde{t}_e))\frac{df}{d\tilde{t}_e}d\tilde{t}_e = n_s(\tilde{t}_e)d\tilde{t}_e \quad \Rightarrow \quad n_{i,s}(\tilde{t}_i) = n_s(f^{-1}(\tilde{t}_i))(\frac{df}{d\tilde{t}_e})^{-1} \tag{41}$$

Where $f^{-1}(x) = y$ is the inverse of $y = f(x)$. The function, f, is not very hard to find using a computer, one simply goes through the entire emission interval, and tabulates the impact times of all short range electrons. Finding an analytical expression however is probably not worth the effort.

The velocity of these short range electrons is given by Eq. (6), and the corresponding impact speed, $\tilde{v}_{i,s}$, is given by changing the sign of this equation, giving

$$\tilde{v}_{i,s} = -\tilde{v}(\tilde{t}_i) = \cos\tilde{t}_e - \alpha - \cos\tilde{t}_i \tag{42}$$

The scheme we use to handle short range impacts and secondary emission is to calculate the impact density for all $\tilde{t}_i$ once per field period, and use it to create secondary electrons with that emission phase. There is however a problem associated with the numerical implementation of this algorithm. The fundamental time scale for the impact statistics of long range electrons is the field period. At the beginning of each period the electrons start from within some height and all impact during one period. We can use the impact distribution to spawn the next generation of long and short range electrons. But the short range electrons have much more complicated trajectories. One short range electron may give rise to several impact-emission events during one period, and tracking this chain of events would destroy the simplicity of our scheme. The effect of only updating the position of the short range electron once every period will be a slowing down of the process with respect to the long range impacts. However, the emitted electrons that will impact almost directly after short range emission will do so with very little energy, corresponding to the emission energy, and will not cause a significant amount of secondary emission. On the other hand, we should not neglect the short range electrons completely, as was done in all the previous non-resonant investigations[23,24,26–28], for some of them will have large impact velocities, and impact in the interval that gives rise to long range electrons. These high velocity electrons take a rather long time between emission and impact (in the order of one period), and we do not disturb the time-evolution significantly by only updating their position once per period.

V. SECONDARY EMISSION

When the long and short range electrons impact the surface, they will spawn a new population of long and short range secondary electrons, n'. The emitted density of secondary electrons from the long range impacts is

$$n'_l(\tilde{t}_i) = \int_{\tilde{v}_{d,\min}}^{\infty} \sigma(\tilde{v}_{i,l})\eta_{i,l}(\tilde{v}_d, \tilde{t}_i)d\tilde{v}_d \tag{43}$$

where σ is the SEY function, which only depends on the impact speed (we disregard any angular variation, as this model does not include any such features).

The secondary emission density caused by impacting short range electrons is

$$n'_s(\tilde{t}_i) = \sigma(\tilde{v}_{i,s})n_{i,s}(\tilde{t}_i) \tag{44}$$

Which means that the total secondary emission during each cycle is

$$n'(\tilde{t}_i) = n'_l(\tilde{t}_i) + n'_s(\tilde{t}_i) \tag{45}$$

This secondary population is divided into a new generation of long and short range electrons having as their emission phase, $\tilde{t}'_e = \tilde{t}_i$. So in a general system where one wants to apply the method above, the impact distributions at any point would have to be related to the emitted secondary distributions at all the other points. In addition to this, there is the complication of time delay between emission at one point and impact at another. Taking account of this leads to the statistical method of Vdovicheva et al.[15]. But restricting ourselves to a steady state, non-resonant scenario, where the average total number of electrons does not change in time, there are two possible situations. Either we have a cyclical evolution of the electron distributions, both in space and time. Luk'yanchikov[24] argues that no such situations occur, but offers no definitive evidence for this. The other, more simple situation is that, at all points, the distribution that is impacting will spawn a perfect copy of itself through secondary emission. Only the latter case will be considered further.

In addition to this simplification we will restrict ourselves to a limited range of geometries. We will consider the two completely analogous cases when we either have two infinite parallel conducting plates that are well separated, or we have one surface to which all emitted electrons are forced to return due to some ponderomotive force. In these two cases, the

electron drift velocity distribution of the incoming and outgoing electrons will be equal but opposite in direction.

In these cases we can apply the results from sections III and IV, specifically using Eqs. (31), (41), (43), and (44) in (45), which gives us the total secondary emission density

$$n'(\tilde{t}_i) = \int_{\tilde{v}_{d,\min}}^{\infty} \sigma(\tilde{v}_{i,l}) \frac{n_l(\tilde{v}_d)}{2\pi\tilde{v}_d}(\tilde{v}_d - \cos\tilde{t}_i)d\tilde{v}_d + \sigma(\tilde{v}_{i,s})n_s(f^{-1}(\tilde{t}_i))(\frac{df}{d\tilde{t}_e})^{-1} \tag{46}$$

In a steady state situation, the incoming long range electrons will have a certain distribution over drift velocity, where the drift velocity is the combined result of the emission velocity and emission phase. Under the assumtion that α is constant, the incoming distribution over drift velocity can be represented by a distribution over emission phase corresponding to the surface it will impact (not the surface which emitted it). Since the drift velocity in these systems is given by

$$\tilde{v}_d = \alpha - \cos\tilde{t}_e \tag{47}$$

The transformation is effected by inserting (47) in (46), replacing $n_l(\tilde{v}_d)d\tilde{v}_d$ with $n_l(\tilde{t}_e)d\tilde{t}_e$, and limiting the integration interval to $[\tilde{t}_{e,\min}, \tilde{t}_{e,\max}]$, resulting in

$$n'(\tilde{t}_i) = \int_{\tilde{t}_{e,\min}}^{\tilde{t}_{e,\max}} \sigma(\tilde{v}_{i,l}) \frac{n_l(\tilde{t}_e)}{2\pi} \frac{\alpha - \cos\tilde{t}_e - \cos\tilde{t}_i}{\alpha - \cos\tilde{t}_e} d\tilde{t}_e + \sigma(\tilde{v}_{i,s})n_s(f^{-1}(\tilde{t}_i))(\frac{df}{d\tilde{t}_e})^{-1} \tag{48}$$

It is necessary to be careful and use the correct limiting times when integrating n_l, because the whole point of the non-resonant approach is to use an average value, where the fact that n_l should be zero outside the allowed interval is not included. The values for $\tilde{t}_{e,\min}$ and $\tilde{t}_{e,\max}$ are given by inserting Eq. (47) in (14) or (15), depending on $\tilde{t}_i$, and solving for $\tilde{t}_e$.

Consider now the new generation of secondaries that will be spawned by the impacting electrons. The density of secondary electrons is given by Eq. (48), and the new electron population is generated by dividing the secondary emission density into a short range and a long range part according to

$$n_s(\tilde{t}_e) = n'(\tilde{t}_e), \quad \tilde{t}_e \in T_S \tag{49}$$

$$n_l(\tilde{t}_e) = n'(\tilde{t}_e), \quad \tilde{t}_e \in T_L \tag{50}$$

where T_S and T_L are the intervals where electrons become short and long range respectively.

In this way we can find a steady state distribution of electrons which represents the electron population on the breakdown threshold simply by finding the combination of parameters which yields a population of secondary electrons which is exactly the same as the incoming one. The equations are possible to solve completely using computer, while analytic solutions can be found for some idealized SEY functions, as well as unrealistically high emission velocities[22].

By setting $\sigma = 1$, we can study the impact dynamics of different distributions over emission phase. It is quite instructive to investigate the impact dynamics of long range electrons having a flat distribution over emission phase ($n_l = N/(\tilde{t}_{e,\max} - \tilde{t}_{e,\min})$, while disregarding the short range electrons. The fraction of impacting electrons that strike in the long range emission interval, and the corresponding average impact speed of these, $\tilde{w}_i$, are shown in Fig. 7 for values of α between 0 and 2. The two most important features of the non-resonant model are seen quite clearly in these figures. The effective SEY of the electrons that impact in the short range emission interval is quite low in comparison with those that impact in the long range interval. In this way, the fraction of impacts in the long range interval, N_L, illustrates the main non-resonant effect; the loss of electrons due to impact in low energy emission regions. The right panel shows quite clearly that the average impact speed is heavily dependent on the emission speed, not only due to the combined velocities, but more importantly due to the size of the long range emission interval, which is very sensitive to α.

VI. REALISTIC, NUMERICAL SOLUTIONS

In this section we shall apply the formalism we developed in the previous sections into calculating the breakdown threshold for realistic systems. It is possible to present the solutions in several ways. For a specific system, where the SEY maximum is known, one can calculate the breakdown threshold for any value of emission energy to first cross over energy ratio. We do this for silver and compare with the predictions of resonant theory, and the approximate value given by Eq. (38).

Besides from calculating the specific threshold for a given SEY maximum, we can calculate the lowest value for the SEY maximum that can sustain multipactor for any combination

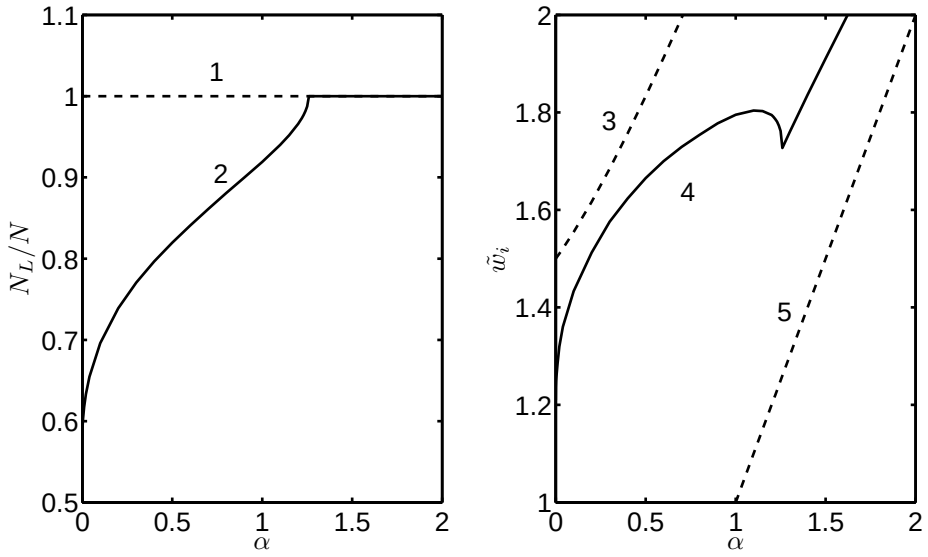

FIG. 7: Line 2 shows the fraction of impacts in the long range emission interval for a flat distribution of electrons over the long range emission phase interval. When $\alpha \approx 1.26$ (see Fig. 2)[15] the entire period is open for long range emission, and the fraction reaches 1, marked by the line 1. Line 4 shows the average impact speed of electrons impacting in the long range emission interval, for a flat electron distribution over the allowed long range emission interval. Line 3 shows the result of Eq. (38), which does not apply for $\alpha < 2$ but is included for reference. Line 5 represents α. The kink in line 4 is due to the rapid expansion of the long range emission interval when α approaches 1.26. This expansion leads to the rapid inclusion of low energy impacts in the interval, and the lowering of the average impact speed.

of emission energy, first cross over energy, and electric field strength. This yields a set of general curves that can be directly applied to any system where some of the parameters are known.

A. The numerical proceedure

To solve the equations using numerical techniques it is necessary to discretize the system. We start with the general equation for the impacting electrons (48)

$$n'(\tilde{t}_i) = \int_{\tilde{t}_{e,\min}}^{\tilde{t}_{e,\max}} \sigma(\tilde{v}_{i,l}) \frac{n_l(\tilde{t}_e)}{2\pi} \frac{\alpha - \cos\tilde{t}_e - \cos\tilde{t}_i}{\alpha - \cos\tilde{t}_e} d\tilde{t}_e + \sigma(\tilde{v}_{i,s}) n_s(f^{-1}(\tilde{t}_i))(\frac{df}{d\tilde{t}_e})^{-1} \qquad (51)$$

It is most convenient to use a fixed time vector for both the emission and impact distributions, on the form

$$\tilde{t}[i] = \frac{\pi}{M}(2i-1), \qquad i = 1...M \tag{52}$$

The time step is $\Delta\tilde{t} = 2\pi/M$. We replace all quantities with their discrete counterparts, and use $\Delta\tilde{t} = \Delta\tilde{t}_i = \Delta\tilde{t}_e$ along with $\tilde{t}_i = \tilde{t}[i]$, and $\tilde{t}_e = \tilde{t}[j]$, to find

$$n'[i] = \frac{1}{M}\sum_{j=j_{\min}}^{j_{\max}} \sigma(\tilde{v}_{i,l}[i,j])n_l[j]\frac{\alpha - \cos\tilde{t}[i] - \cos\tilde{t}[j]}{\alpha - \cos\tilde{t}[j]} + \sigma(\tilde{v}_{i,s}[i,j_s[i]])n_s[j_s[i]] \tag{53}$$

where $\tilde{t}[i] = f[\tilde{t}[j_s[i]]]$, and the number density of emitted electrons at $\tilde{t}[i]$ is $n'[i]$. The complete removal of the inverse derivative appearing with the short range electron density is a practical measure. Since we are using time vectors with the same step size for $\tilde{t}_i$ and $\tilde{t}_e$, the discretization of $\tilde{t}_i = f(\tilde{t}_e)$ will result in a situation where each impact time will not have a corresponding emission time, and to ensure the conservation of particle number, the simplest solution is to put $(df/d\tilde{t}_e)^{-1} = 1$. This entire proceedure results in a certain jaggedness of the resulting short range impact density, which can be reduced by using a fine time vector, i.e. a large M.

Finding a solution, and the breakdown threshold, for a given SEY-function consists of balancing the number of electrons in the incoming distribution, $n_l + n_s$, with the electrons in the secondary emission distribution, n'.

B. Solutions

How to express the solution depends on the choice of SEY-function. The most simple Vaughan model[31], Eq. (54), has two parameters that determine its shape; the maximum SEY, $\sigma_{\max}$, and the first cross over energy, W_1 (or equivalently the SEY maximum energy, $W_{\max}$).

$$\sigma = \sigma_{\max}\left[\epsilon\exp(1-\epsilon)\right]^{\beta} \tag{54}$$

where $\epsilon = W_i/W_{\max} = (v_i/v_{\max})^2$, $\beta = 0.62$ for $\epsilon < 1$, and 0.25 for $\epsilon \geq 1$. To fix the problem completely, one also has to know the emission energy of the secondary electrons, W_e, and

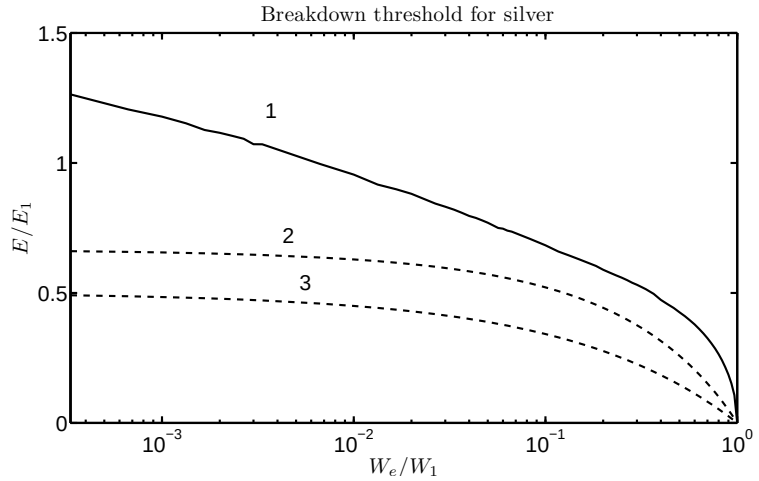

FIG. 8: On the ordinate axis, the breakdown field amplitude, E, divided by the amplitude corresponding to the electron oscillatory velocity being equal to the first cross over velocity, $E_1 = m\omega v_1/e$. On the abscissa axis, the emission energy, W_e, divided by the first cross over energy, W_1. Line 1 shows the breakdown field according to the numerical solution of the non-resonant model. Line 2 corresponds to the non-resonant approximation, $((v_\omega + v_e)^2 + v_\omega^2/2)/(v_\omega + v_e) = v_1$, whereas line 3 corresponds to the resonant approximation, $2v_\omega + v_e = v_1$.

the frequency of the electric field. Given these four parameters, there is only one value for the electric field amplitude, E_0, which will result in an equilibrium distribution function.

The threshold for silver, found from solving Eq. (53), is shown in Fig. 8. Silver has $W_1 = 30$ eV, and $\sigma_{\max} = 2.22$[29,30,32], and the act of solving for the breakdown threshold consists in finding the electric field strength ratio E_0/E_1 which produces a steady state impact-emission density for a given ratio W_e/W_1. The two dashed lines indicate the approximations corresponding to non-resonant (Eq. (38)), $v_1 \approx ((v_\omega + v_e)^2 + v_\omega/2)/(v_\omega + v_e)$, and resonant multipactor, $v_1 \approx 2v_\omega + v_e$ (see Kryazhev et al.[25] for a discussion on this topic). It is seen quite clearly that these approximations are only good for rather high emission velocities. The non-resonant approximation is closer to the numerical value since it takes account of the fact that the impact speed is a statistical average, but it fails to include the heavy dependance of the size of the short range interval upon the emission velocity. This leads to an underestimation of the threshold field for low values of the emission velocity. The failure of the resonant approximation is due to the compound effect of the loss of electrons into the short range intervals, and the assumption that all electrons participating in the discharge impact with the maximal velocity.

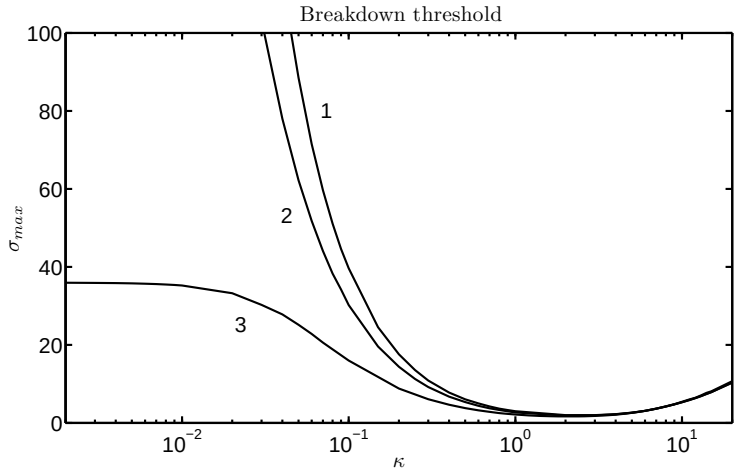

FIG. 9: Universal non-resonant breakdown curves for the simple Vaughan SEY function. The left hand branch corresponds to the lower breakdown threshold, and the right hand branch to the upper threshold. The SEY maximum on the y-axis is allowed to reach unrealistic values to illustrate the functional behavior. The values for γ are 0.001, 0.01 and 0.1 for lines 1, 2 and 3.

We now wish to construct more general curves that describe the breakdown threshold for any system, given the shape of the SEY function. Grishin and Luk'yanchikov[26] constructed a set of such curves by using nondimensional variables. They used a different model for the SEY than the standard curve nowadays, so our choice of dimensionless variables is slightly different, but their main conclusions were correct. First of all they concluded that given the shape of the SEY curve, one can find a set of dimensionless parameters, that will provide a universal set of curves, describing the necessary criterion for non-resonant multipactor. We use the most simple form of the Vaughan model, and the most logical choice for the dimensionless parameters seems to be, $\gamma \equiv v_e/v_1$, $\kappa \equiv v_\omega/v_1$, and $\sigma_{\max}$. By using these parameters when solving Eq. (53), we can find a set of curves which allows one to determine the critical regions for multipactor in general. These curves are shown in Figs. 9 and 10.

The left hand branch of these curves depict the lower threshold and the dependence on the emission velocity. In the limit where $\gamma = 1$ the threshold reaches a value $\sigma_{\max} = 1$, and any small decrease in γ causes a very steep increase in the limiting value for $\sigma_{\max}$ as $\kappa \to 0$. Previous investigations have shown that there is a lower value of $\sigma_{\max}$ for the existence of non-resonant multipactor. Fig. 10 illustrates quite clearly that this value is heavily dependent on the emission velocity. For the special case when $\gamma = 0$ we find the smallest value of $\sigma_{\max}$ to be roughly 1.97, which is remarkably close to the value 1.96 found

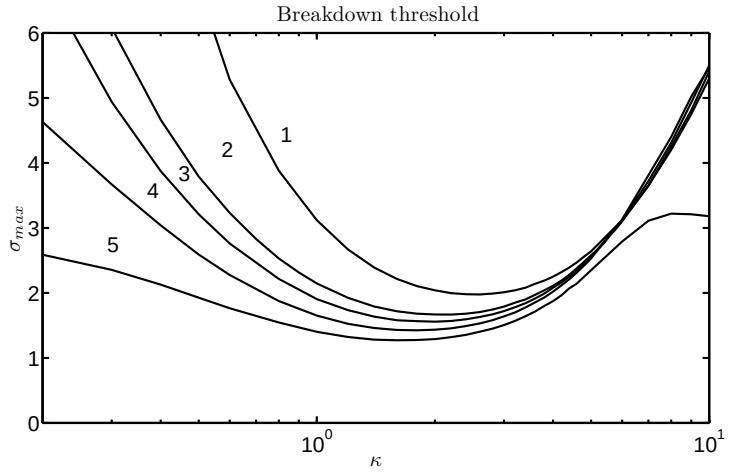

FIG. 10: More realistic values for the SEY maximum and fractions $\gamma = 0$, 0.1, 0.2, 0.4 and 0.8 for curves 1 to 5.

by Grishin and Luk'yanchikov[26]. The values should be close, for they used a SEY curve not too far from Vaughan's, but the almost exact agreement is likely to be a coincidence. It should be noted however that $\gamma = 0$ is unrealistic, and more realistic values of γ should be roughly in the range 0.1-0.5, depending on the material. It is more difficult to compare our results with Sazontov et al.[17], for they do not state explicitly at what fraction v_ω/v_1 the limiting values for the SEY were found. It is also difficult to compare with the values of Kossyi et al.[28] and Sakamoto et al.[33], for in the first case there is the presence of a DC field to account for, and in the second case, the model for secondary emission is rather different. Suffice to say, our investigations are not in contradiction with any of these results, for in our model, any value of the threshold SEY between 1.97 and 1 can be found.

On the right hand branch of the figures we find the upper threshold. In this region the multipactor avalanche takes on quite a different dynamical structure than that which we have previously assumed. In this case it is the low energy impacts that will have a high SEY. Only a small fraction of the long range electrons will make low energy impacts, and thus generate a net increase in electrons. For realistic values of γ, these electrons will be emitted in the short range interval, and must first make a low energy impact in the long range interval before any new long range electrons are generated. The method we have developed in this paper is ill suited for investigating this type of multipactor, for we have simplified the short range dynamics significantly. Due to this fact, only a short segment of the line corresponding to the upper threshold is included in the figures.

VII. COMPARISON WITH SIMULATIONS

We wish to compare our model with simulations, to verify that the statistical treatment is correct and gives good predictions. In order to do this we created a Monte Carlo code which simulates the electron trajectories in a parallel plate system. The full non-resonant regime is hard to reach in simulations, for it is necessary to run the code for so many cycles, with such a large gap, that statistical fluctuations in the electron population becomes overwhelming. However, it is not necessary to reach the full non-resonant regime, for the important characteristics should become evident much earlier (as is suggested by Fig. 5), and it is merely the removal of resonant artefacts which is achieved by going to the limit. The scheme of the Monte Carlo code was rather simplistic. The trajectories of the electrons in the system are known exactly, and the stochastic part of the program consisted of the electron emission velocity, which was randomly distributed, using a flat distribution, in an interval $v_e \in [0.5v_{e,0}, 1.5v_{e,0}]$, where $v_{e,0} = \sqrt{2W_e/m}$, and W_e is the emission energy. The field period was divided into M segments, where $M \geq 200$ was found to give sufficient accuracy. Each phase segment contained T electron trajectories, where the necessary number of trajectories needed to suppress random fluctuations in the result depended on the number of field periods considered in the simulation. A value of at least $T = 100$ was found to be necessary. During the first cycle, all $M \times T$ trajectories where launched from the lower plate, and the impact statistics on the upper and lower plate was recorded, together with the total number of electrons. During the first cycle, each trajectory contained one electron, but upon impact, this number was multiplied with the secondary emission yield corresponding to the impact speed of the trajectory. The multipactor threshold was defined as the point where the total electron number started to show an exponential increase over the main part of the total simulation time. The total amount of time it was necessary to run the code also depended on the gap size, but at least a 100 field periods was used. Running the code for too long causes the electron population to develop a randomly fluctuating sequence. After a while, depending on the number of trajectories included in the code, some electron trajectories will grow wildly due to a sequence of high emission impacts, but then upon the next impact, the impact phase might be in a region of very low secondary emission, and the trajectory is depleted of electrons completely. In this way, the total population of electrons will suffer random depletion, eventually stopping the avalanche completely, even

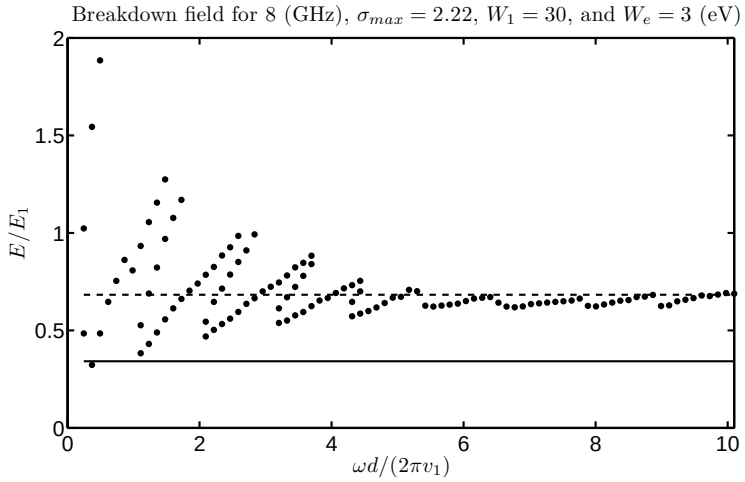

FIG. 11: The breakdown threshold for a parallel plate gap with silver surfaces. The dashed line shows the predictions by the non-resonant theory, whereas the solid line represents the identity $2v_\omega + v_e = v_1$.

though the field might be above the breakdown threshold. It is therefore very important to be wary of this random electron depletion, not mistaking it for subthreshold behavior, and counteracting it by increasing the number of trajectories.

The parameters used in the simulations were $\sigma_{\max} = 2.22$, $W_e = 3$ eV, $W_1 = 30$ eV, $f = 8$ GHz, and d going between 0.1 and 4.1 mm in steps of 0.05 mm. The choice of parameters corresponds to silver, and is the same as in our previous recent publications[29,30], making the results easy to compare. But as is seen in Fig. 11, the threshold can be presented in a normalized way, against a normalized gap width, making the solution applicable to other frequencies and gaps where the SEY and emission velocity characteristics are the same. As stated, Fig. 11 shows the breakdown threshold for the case of silver surfaces as a function of normalized gap width. For small gaps, the resonant structure is evident, and even the first hybrid resonance zone can be seen. But as the gap width is increased, the resonance is suppressed quite rapidly. It is quite clear that the breakdown threshold predicted by the non-resonant theory is very close to the simulated one, except in the regions where some resonant behavior can be seen.

Fig. 12 displays the electron impact distribution on one of the parallel plates for three gap widths, when the field is slightly below the threshold. The two smallest gap widths correspond to the first and second resonance zones, whereas the large gap width correspond to the beginning of the non-resonant regime. Clearly, the emission velocity spread coupled

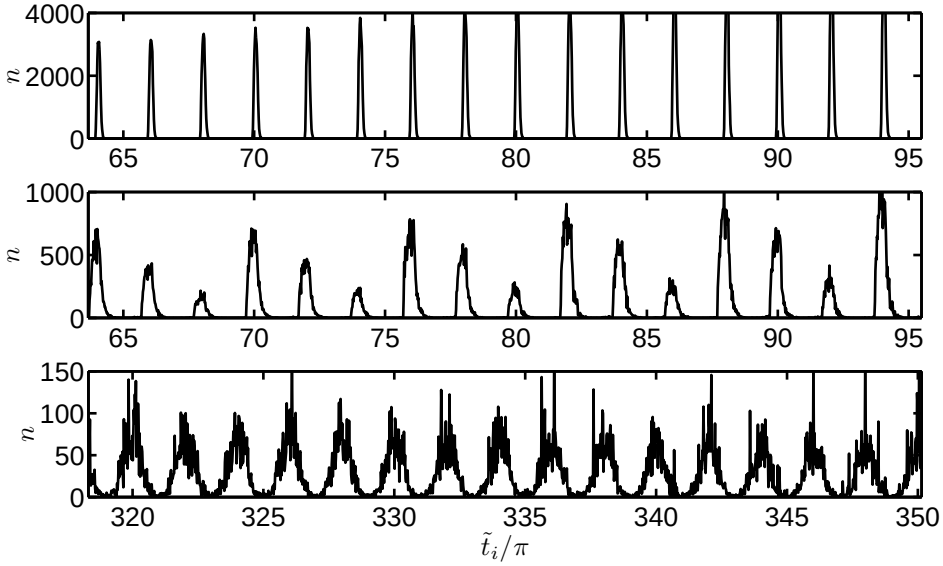

FIG. 12: The impact distributions on the breakdown threshold for three different gap widths: $d = 0.15$, 0.45 and 6 mm, from top to bottom, using 20000, 20000 and 150000 trajectories respectively. The field frequency is 8 GHz, the voltages 150, 450 and 3500 respectively, and the surface parameters correspond to silver. The smallest gap width corresponds to the first resonance zone, the intermediate gap width to the second resonance zone, and the largest gap width represents the situation close to the non-resonant regime. It is clear that for the smallest gap, the emission velocity spread causes little disturbance to the impact phase distribution, whereas for the intermediate gap, the influence starts to show. For the largest gap width, impacts are distributed in a sinusoidal pattern over the entire field period.

with the transit time determines the overall impact distribution. For the smallest gap, electrons impact only in a very narrow region, whereas for the second resonance zone, this region has expanded. For the largest gap, the distribution appears sinusoidal, which agrees qualitatively with the non-resonant predictions (see Fig. 6).

VIII. CONCLUSIONS

The main purpose of the statistical treatment in this paper has not been to describe any new physics, but rather to point the direction to a faster way of finding the multipactor threshold in complicated systems where simulations are impractical, and a full statistical treatment might be very complicated. At the present stage of development, the theory

should be directly applicable to finding the threshold in a parallel plate geometry with a large gap, a coaxial waveguide with a small inner conductor excited in the TE_{01} mode, and a circular waveguide excited in the TM_{01} mode. Proving beyond doubt that the model is working for all such cases where the multipactor avalanche can be considered as non-resonant is of course impossible. Instead a comparison between the model and simulations has been done in the important case of parallel plates with a large separation. The predicted and simulated breakdown threshold fields are in agreement, and the impact statistics show the same qualitative behavior in theory and simulations. In addition to this, general curves for the non-resonant threshold have been found for the simple Vaughan approximation for the SEY. It was seen that there is a lower value of the SEY maximum under which non-resonant multipactor is impossible, but that the actual value is heavily dependent on the emission velocity, and can be anywhere between 1 and 1.97. The general mechanisms for the raising of the lower multipactor threshold has been identified as the lowering of the average electron impact speed and the loss of electrons into phase regions of low secondary emission. Both these effects are due to the statistical impact spread of electrons, essentially caused by the spread in emission velocity coupled with long transit times. As for the upper threshold, it was realized that a discharge close to the threshold must be of a quite different nature as compared to the one typically considered. Instead of high energy electrons causing emission of high energy electrons with large drift velocities, it is the low energy impacts of high energy electrons that are able to sustain multipactor, through impacts in the short range interval, where in turn, those secondaries will impact in the long range interval. Evidently, this type of multipactor is rather complicated, and the statistical nature of the secondary emission is very important. As a consequence, it cannot be accurately modeled with the methods used in this paper, and it is unclear as to whether this mechanism is actually physically realizable.

---

[1] R. A. Kishek, Y. Y. Lau, L. K. Ang, A. Valfells, and R. M. Gilgenbach, Multipactor discharge on metals and dielectrics: Historical review and recent theories, *Phys. Plasmas*, **5**, 5, 2120 (1998).

[2] J. R. Vaughan, Multipactor, *IEEE Trans. Electron Dev.*, **35**, 7, 1172 (1988).

[3] A. J. Hatch, and H. B. Williams, The Secondary Electron resonance Mechanism of Low-Pressure High-Frequency Gas Breakdown, *J. Appl. Phys*, **25**, 4, 417 (1954).

[4] A. J. Hatch, and H. B. Williams, Multipacting Modes of High-Frequency Gaseous Breakdown, *Phys. Rev.*, **112**, 3, 681 (1958).

[5] V. E. Semenov, E. Rakova, R. Udiljak, D. Anderson, M. Lisak, and J. Puech, Conformal mapping analysis of multipactor breakdown in waveguide irises, *Phys. Plasmas*, **15**, 3, 033501 (2008).

[6] A. G. Sazontov, V. A. Sazontov, and N. K. Vdovicheva, Multipactor breakdown prediction in a rectangular waveguide, *Contrib. Plasma Phys.*, **48**, 4, 331 (2008).

[7] V. E. Semenov, E. I. Rakova, D. Anderson, M. Lisak, and J. Puech, Multipactor in rectangular waveguides, *Phys. Plasmas*, **14**, 3, 033501 (2007).

[8] V. E. Semenov, E. Rakova, N. Zharova, D. Anderson, M. Lisak, and J. Puech, Simulations of the multipactor effects in hollow waveguides with wedge-shaped cross section, *IEEE Trans. Plasma Sci.*, **36**, 2, 488 (2008).

[9] J. Hueso, C. Vicente, B. Gimeno, V. E. Boria, S. Marini, and M. Taroncher, Multipactor effect analysis and design rules for wedge-shaped hollow waveguides, *IEEE Trans. Electron Dev.*, **57**, 12, 3508 (2010).

[10] R. Udiljak, D. Anderson, M. Lisak, V. E. Semenov, and J. Puech, Multipactor in a coaxial transmission line. I. Analytical study, *Phys. Plasmas*, **14**, 033508 (2007).

[11] A. M. Perez, C. Tienda, C. Vicente, A. Goves, G. Torregrosa, B. Gimeno, R. Barcot, V. E. Boria, and D. Raboso, Multipactor analysis in coaxial waveguides for satellite applications using frequency-domain methods, *IEEE MTT-S Int. Microw. Symp. Dig.*, 1045-1048 (2006).

[12] V. E. Semenov, N. Zharova, R. Udiljak, D. Anderson, M. Lisak, and J. Puech, Multipactor in a coaxial transmission line. II. Particle-in-cell simulations, *Phys. Plasmas*, **14**, 3, 033509 (2007).

[13] A. M. Perez, C. Tienda, C. Vicente, S. Anzam, J. Gil, B. Gimeno, V. E. Boria, and D. Raboso, Prediction of multipactor breakdown thresholds in coaxial transmission lines for travelling, standing, and mixed waves, *IEEE Trans. Plasma Sci.*, **37**, 10, 2031 (2009).

[14] V. E. Semenov, N. A. Zharova, D. Anderson, M. Lisak, and J. Puech, Simulations of multipactor in circular waveguides, *Phys. Plasmas*, **17**, 2, 123503 (2010).

[15] N. K. Vdovicheva, A. G. Sazontov, and V. E. Semenov, Statistical theory of two-sided multipactor, *Radiophys. Quantum Electron.*, **47**, 8, 580 (2004).

[16] N. K. Vdovicheva, A. G. Sazontov, V. A. Sazontov, and V. E. Semenov, Influence of the angular anisotropy of secondary emission on the characteristics of two-sided multipactor, *Radiophys.*

Quantum Electron., **49**, 5, 368 (2006).

[17] A. Sazontov, M. Buyanova, V. Semenov, E. Rakova, N. Vdovicheva, D. Anderson, M. Lisak, J. Puech, and L. Lapierre, Effect of emission velocity spread of secondary electrons in two-sided multipactor, *Phys. Plasmas*, **12**, 053102 (2005).

[18] S. Anza, C. Vicente, J. Gil, V. E. Boria, B. Gimeno, and D. Raboso, Nonstationary statistical theory for multipactor, *Phys. Plasmas*, **17**, 062110 (2010).

[19] A. G. Sazontov, V. A. Sazontov, and N. K. Vdovicheva, Multipactor Breakdown Prediction in a Rectangular Waveguide: Statistical Theory and Simulation Results, *Contrib. Plasma Phys.*, **48**, 4, 331 (2008).

[20] A. Sazontov, V. Semenov, M. Buyanova, N. Vdovicheva, D. Anderson, M. Lisak, J. Puech, and L. Lapierre, Multipactor discharge on a dielectric surface: Statistical theory and simulation results, *Phys. Plasmas*, **12**, 093501 (2005).

[21] S. Anza, M. Mattes, C. Vicente, D. Raboso, V. E. Boria, and B. Gimeno, Multipactor theory for multicarrier signals, *Phys. Plasmas*, **18**, 032105 (2011).

[22] J. F. Johansson, and J. Rasch, Non-Resonant Probabilistic Multipactor Calculations, Mulcopim, September 21-23, Valencia, Spain (2011).

[23] V. A. Stanskii, D. A. Ganichev, and S. A. Fridrikhov, Calculation of the effective coefficient of secondary electron emission from walls localizing a microwave discharge, *Sov. Phys. Tech. Phys.*, **18**, 8, 1103 (2007).

[24] G. S. Luk'yanchikov, Multiphase, uniform, secondary-emission microwave discharge at a solid surface, *Sov. Phys. Tech. Phys.*, **19**, 9, 1196 (1975).

[25] A. Kryazhev, M. Buyanova, V. Semenov, D. Anderson, M. Lisak, J. Puech, L. Lapierre, and J. Sombrin, Hybrid resonant modes of two-sided multipactor and transition to the polyphase regime, *Phys. Plasmas*, **9**, 11, 4736 (2002).

[26] L. V. Grishin, and G. S. Luk'yanchikov, Multipactor discharge with an electron velocity distribution, *Sov. Phys. Tech. Phys.*, **21**, 3, 307 (1976).

[27] A. A. Dorofeyuk, I. A. Kossyi, G. S. Luk'yanchikov, and M. M. Savchenko, Electron discharge in the interaction of microwave radiation with a metal surface, *Sov. Phys. Tech. Phys.*, **21**, 1, 76 (1976).

[28] I. A. Kossyi, G. S. Luk'yanchikov, V. E. Semenov, E. I. Rakova, D. Anderson, M. Lisak, and J. Puech, Experimental Study of the Single-Surface Poly-Phase Multipactor on a Metal Plate,

Mulcopim, September 21-23, Valencia, Spain (2011).

[29] J. Rasch, D. Anderson, J. F. Johansson, M. Lisak, J. Puech, E. Rakova, and V. E. Semenov, Microwave Multipactor Breakdown Between Two Cylinders, *IEEE Trans. Plasma Sci.*, **38**, 8, 1997 (2010).

[30] J. Rasch, V. E. Semenov, E. Rakova, D. Anderson, J. F. Johansson, M. Lisak, and J. Puech, Simulations of Multipactor Breakdown Between Two Cylinders, *IEEE Trans. Plasma Sci.*, **39**, 9, 1786 (2011).

[31] J. R. Vaughan, A New Formula for Secondary Emission Yield, *IEEE Trans. Electron Dev.*, **36**, 9, 1963 (1989).

[32] *Space Engineering, Multipactor Design, and Test*, ECSS-E-20-01-01A, May 5 (2003).

[33] K. Sakamoto, Y. Ikeda, and T. Imai, Numerical study of RF discharge caused by secondary electron emission, *J. Phys. D: Appl. Phys.*, **22**, 1841 (1989).